Journal of Catalysis **202,** 279–295 (2001)
doi:10.1006/jcat.2001.3304, available online at http://www.idealibrary.com on IDEAL®

Alumina-Supported Copper Chloride

3. Effect of Exposure to Ethylene

G. Leofanti,*,[1] A. Marsella,* B. Cremaschi,* M. Garilli,* A. Zecchina,‡ G. Spoto,‡ S. Bordiga,‡ P. Fisicaro,‡ G. Berlier,‡ C. Prestipino,‡ G. Casali,‡ and C. Lamberti†,‡,[2]

*European Vinyls Corporation Italia, Inovyl Technological Centre, Via della Chimica 5, 30175 Porto Marghera (Venezia), Italy; †Unità INFM Torino-Università, Torino, Italy; and ‡Dipartimento di Chimica Inorganica, Chimica Fisica e Chimica dei Materiali, Università di Torino, Via P. Giuria 7, 10125 Torino, Italy

Received January 22, 2001; revised June 7, 2001; accepted June 11, 2001

The effect of exposure to C_2H_4 of different $CuCl_2/Al_2O_3$ catalysts characterized by a wide copper content (0.25 < Cu wt% < 9.0) has been discussed. X-ray absorption near edge spectroscopy, electron spin resonance, and near infrared diffuse reflectance spectroscopy (NIR DRS) techniques and IR spectroscopy of adsorbed NO and CO, have been used to demonstrate that the key mechanism of the oxychlorination reaction is the reduction of $CuCl_2$ to CuCl following the path $2CuCl_2 + C_2H_4 \rightarrow C_2H_4Cl_2 + 2CuCl$. This reaction holds for the cupric ions in the supported amorphous $CuCl_2$ phase, with its activity enhanced by a very high degree of dispersion as demonstrated by chemisorption measurements (up to 72%). In contrast Cu(II) cations forming the surface copper aluminate phase are unreactive toward ethylene. A detailed analysis of the IR spectra obtained at liquid nitrogen temperature allows extraction of important information on catalyst support: (i) Cl^- anions are hosted on the support surface and their presence enhances the Brønsted acidity of the surface >Al–OH groups; and (ii) $>Al^{3+}$ coordinative unsaturated Lewis acidic sites are present on the catalyst. These results point out the possible determinant role of the support in side reactions and coking that are responsible for loss of selectivity and, respectively, catalyst decay during industrial runs.

Key Words: **Al_2O_3-supported $CuCl_2$; ethylene oxychlorination; XANES; EPR; IR spectroscopy; CO chemisorption.**

1. INTRODUCTION

This paper represents the third part of a series devoted to the investigation of $CuCl_2$ supported on γ-alumina, the base catalyst for ethylene oxychlorination. In the two previous works (1, 2), a set of $CuCl_2/Al_2O_3$ catalysts has been prepared in a wide range (0.25–9 Cu wt%) of Cu concentration and characterized using several techniques (UV–vis spectroscopy, solubility tests, electron spin resonance (EPR), extended X-ray absorption fine structure (EXAFS), and X-ray diffraction (XRD)). In those studies, the following objectives have been achieved (1–3): (i) identification of the species present at different Cu loading; (ii) determination of their concentration; and (iii) investigation of mutual transformations during impregnation, aging, and heating treatments up to the typical oxychlorination temperature (500–550 K).

The first paper (1), concerning freshly prepared samples (i.e., 1 h after impregnation), reached the following conclusions: (i) at copper content lower than 0.95 wt% Cu per 100 m^2 support, a Cu surface aluminate phase takes place where the copper ions are surrounded only by 5 oxygen ligands at 1.92 Å; (ii) chlorine released by $CuCl_2$ during its interaction with alumina gives >Al–Cl species; and (iii) once the adsorptive capacity of alumina is exhausted (which occurs for copper content greater than 0.95 wt% Cu per 100 m^2 support), copper chloride precipitates directly from the solution with the formation of $CuCl_2 \cdot 2H_2O$.

In the second paper (2), the effect of aging and heating on the structure of the species discussed previously has been examined, resulting in the following main points: (i) surface Cu-aluminate is stable under both aging and heating treatments; (ii) $CuCl_2$ undergoes a slow hydrolysis with formation of paratacamite; (iii) HCl released during hydrolysis reacts with alumina with formation of >Al–Cl species, ensuring a Cl/Cu ratio of 2 along all the aging processes; (iv) while heating, the alumina partially releases the chlorine fixed to the surface, resulting in the reverse transformation of paratacamite into copper chloride; (v) in the oxychlorination reaction conditions, paratacamite is absent and only surface aluminate and copper chloride (or products arising from the interaction of these compounds with reactants or reaction products) are present in the catalyst; and (vi) surface copper aluminate is inactive and ethylene conversion is proportional to the amount of $CuCl_2$, which has been identified as the active phase.

[1] Present address: Via Firenze 43, 20010 Canegrate (Milano), Italy.
[2] To whom correspondence should be addressed. Fax: 39-011-6707855. E-mail: Lamberti@ch.unito.it.

0021-9517/01 $35.00

This third work, which is devoted to investigating the catalyst after interaction with C_2H_4, is structured into four parts. In the first part (Section 3.1) it is shown that interaction with ethylene is able to reduce $CuCl_2$ to a new Cu(I) phase, although it does not modify the Cu aluminate phase. In the second part (Section 3.2) it is demonstrated that the reduced Cu(I) phase is CuCl. The third part (Section 3.3) is devoted to a study of the dispersion of the CuCl phase, while in the last part (Section 3.4) the surface of the support is characterized to investigate if other sites rather than the Cu(I)/Cu(II) red-ox-couple of $CuCl/CuCl_2$ are available for reagents and products.

Coming to the first two points, let us recall that the overall oxychlorination reaction

$$C_2H_4 + 2HCl + 1/2\ O_2 \rightarrow C_2H_4Cl_2 + H_2O, \qquad [1]$$

is supposed to occur in three subsequent steps (4–9): (i) reduction of $CuCl_2$ into CuCl by ethylene; (ii) reoxidation of CuCl by oxygen; and (iii) closure of the loop, by restoration of the original $CuCl_2$, with HCl as described in Eqs. [2–4]:

$$2CuCl_2 + C_2H_4 \rightarrow C_2H_4Cl_2 + 2CuCl, \qquad [2]$$

$$2CuCl + 1/2\ O_2 \rightarrow Cu_2OCl_2, \qquad [3]$$

$$Cu_2OCl_2 + 2HCl \rightarrow 2CuCl_2 + H_2O. \qquad [4]$$

Obviously the working catalyst simultaneously undergoes three different reactions described in Eqs. [2–4]. However, to simplify the characterization and to avoid any ambiguity in the interpretation of the results, we will study the effect of the three steps separately. The investigation of the first step (Eq. [2]) is presented in Sections 3.1 and 3.2 of this work, while the oxidation and rechlorination steps (Eqs. [3] and [4]) will be the core of a subsequent manuscript (10).

Of course, the validity of our approach is subordinated to the assumption that the actual reaction path can be really divided into the three substeps. In fact, no experimental evidence has been reported so far, and the substeps [2–4] have been presented on a theoretical ground only in the quoted references (4–9). In this work and in the subsequent one (10) we will bring the experimental proof that steps [2–4] represent a possible effective reaction path, although *a posteriori* our approach will so be justified.

2. EXPERIMENTAL

2.1. Materials

$CuCl_2/Al_2O_3$ catalysts, characterized by a Cu loading ranging from 0.25 to 9.0 wt%, were prepared by impregnation of γ-allumina (Condea Puralox SCCa 30/170; surface area: 168 $m^2\ g^{-1}$, pore volume: 0.50 $cm^3\ g^{-1}$) with an aqueous solution of $CuCl_2 \cdot H_2O$ following the incipient wetness method (1). According to the convention adopted in Refs. (1, 2) the copper content is used to identify the samples: for example Cu9.0 indicates the sample containing 9.0 wt% Cu.

To help with the interpretation of results, a few additional samples have been prepared ad hoc: (i) the unimpregnated γ-alumina; (ii) the chlorinated γ-alumina [obtained after interaction of support with HCl: 1.8 wt%, corresponding to the maximum amount of Cl which can be released as an effect of copper aluminate formation; see Ref. (1)]; (iii) an unimpregnated ($\theta + \alpha$)-alumina (32 $m^2\ g^{-1}$); (iv) an unimpregnated α-alumina (7.1 $m^2\ g^{-1}$); (v) 5.0 wt% Cu samples supported on the α-alumina; and (vi) sample CuO5.0. This last sample was prepared by impregnation of the γ-alumina with an aqueous solution of $Cu(NO_3)_2 \cdot 2H_2O$ following the incipient wetness method (1). After impregnation the CuO5.0 sample was dried at 310 K under air flow for 1 h and then calcined at 673 K to decompose the nitrate. In analogy with the convention already adopted for samples prepared from $CuCl_2$, the number 5.0 indicates the wt% copper concentration.

2.2. Methods

EPR spectra have been measured at liquid nitrogen temperature (LNT) on a Varian E 109 spectrometer equipped with a dual cavity and operating in the X band. Varian Pitch has been used as a reference for the calibration of g values. Before cooling, samples have been evacuated at room temperature (RT) up to 10^{-3} Torr (1 Torr $\approx$ 133.3 Pa).

X-ray absorption measurements were carried out using synchrotron radiation of the EXAFS13 station at LURE (Orsay, France) during experiment CK017-00 (11). Both EXAFS and X-ray absorption near edge spectroscopy (XANES) measurements were carried out in transmission mode using air-filled ionization chambers for both incident and transmitted beams. The former was monochromatized using a Si(111) or a Si(331) channel-cut monochromator for EXAFS and XANES spectra, respectively. EXAFS (XANES) spectra have been collected with a sampling step of 2.0 (0.5) eV/point and an integration time of 2 (1) s/point. Four EXAFS spectra were recorded in the same experimental conditions for each sample. $\chi(k)$ extraction and EXAFS data analysis have been performed using programs developed by Michalowicz (12), following standard procedures (13), as described in detail in Ref. (14). The Cu–Cl and Cu–O phase shift and amplitude functions have been extracted from anhydrous $CuCl_2$ (4 equivalent chlorine atoms at 2.26 Å (15)) and from CuO_2 (4 equivalent oxygen atoms at 1.85 Å (16)) model compounds, respectively.

For infrared (IR) measurements, a thin self-supporting pellet of the catalyst was prepared and activated under dynamic vacuum at 500 K for 2 h inside an IR cell designed to allow *in situ* temperature treatments, gas dosage (CO and NO), and low-temperature measurements. The IR spectra were recorded at 2 cm^{-1} resolution on a BRUKER FTIR 66

spectrometer equipped with a mercury cadmium telluride cryodetector. As far as CO is concerned, the optical isotherms at LNT will be reported. Upon NO dosage at LNT too low a P_{NO} is obtained ($\sim 7 \times 10^{-2}$ Torr). Spectra have been so recorded during the successive gradual warming to RT. At the first stages (up to about 150 K) the IR bands increase due to the abrupt increase of P_{NO}, while at higher temperatures NO starts a desorbing process from the surface sites resulting in a decrement of the corresponding IR bands. For graphical reasons the IR spectra of adsorbed NO reported in this work concern only the first stages (i.e., from LNT up to the maximum coverage spectrum). It is worth noting that no further information can be extracted from the omitted spectra.

Static-volumetric CO adsorption measurements were made by a Micromeritics ASAP 2010C device equipped with a turbomolecular pump, which allowed us to obtain a vacuum better than 10^{-5} Torr in the sample holder. All the treatments, including adsorption, were performed with sufficient time to reach equilibrium. The pretreatment consisted of an evacuation at 308 K for 5 min, an evacuation at 500 K for 0.5 h, five cycles of reduction with ethylene at 200 Torr at 500 K for 15 min followed by evacuation at the same temperature for 15 min (the last time for 60 min), and at last an evacuation at 308 K for 30 min. The adsorption measurements were made with CO at 308 K. They consisted of the determination of the isotherms in the 10^{-4}–600 Torr range (about 20 min per point). A Perkin-Elmer Lambda 15 spectrofotometer, equipped with an integrating sphere, has been used to perform the NIR DRS measurements.

3. RESULTS AND DISCUSSION

3.1. Reducibility of Copper Species on Exposure to Ethylene at 500 K

This section concerns elucidation of the behavior of the alumina-supported $CuCl_2$ catalyst on exposure to C_2H_4 at the oxychlorination reaction temperature. According to this approach, the reference sample must be the activated catalyst (i.e., the sample heated up to the typical oxychlorination temperature (in this study 500 K) before exposure to reagents). Activation of the industrial catalyst is done under the flux of inert N_2, while due to technical reasons all samples observed in this study have undergone an activation treatment under vacuum conditions.

As reviewed in (1, 2), it is widely recognized that all copper species present in the catalyst before the thermal treatment should be in the oxidation state of +2. However, we have observed that a thermal treatment up to 500 K, under vacuum conditions, implies a partial reduction of Cu(II) to Cu(I) species similar to that observed on Cu(II)-exchanged zeolites (17–20). The entity of the reduction depends on the adopted vacuum system (both pumps and apparatus), the heating ramp, and the time at 500 K. To verify the correspondence of results between the lab-scale and the industrial activation procedures, an IR measurement of adsorbed CO at RT, in which response is proportional to the amount of available surface Cu(I) ions (*vide infra*; Section 3.3.1), has been performed on Cu9.0 samples previously activated at 500 K both in N_2 flux and under vacuum. The results obtained (not reported for brevity) indicate that the fraction of cuprous ions found after activation in N_2 is negligible, with respect to the fraction found on a similar sample activated *in vacuo* using the same thermal ramp. Notwithstanding this, after reduction in ethylene, IR spectroscopy of adsorbed CO shows the same spectra, reflecting the same amount of surface Cu(I) ions, independent of the adopted activation procedure. This preliminary study allows activation of all samples under vacuum conditions, which represents a considerable simplification of the experimental procedure.

3.1.1. IR study of adsorbed NO. NO is a suitable probe molecule to investigate the oxidation state of surface copper species because it adsorbs on both cuprous and cupric sites (14, 21, 22). The IR spectra of NO dosed at LNT on the Cu4.6 sample activated *in vacuo* at 500 K before and after interaction with ethylene are reported in Fig. 1 as a function of the increase of the sample temperature from LNT up to the maximum coverage spectrum (see Section 2). The starting spectrum of both experiments reports the system at LNT, where a single component is observed at 1885 cm^{-1} (strong in Fig. 1a and weak in Fig. 1b). From the literature, this band is ascribed to Cu(II) ... NO complexes (14, 21, 22). We observe that the exposure of sample to ethylene causes a strong decrease of cupric cations detected by NO adsorption. The rather large FWHM suggests a considerable heterogeneity of the cupric adsorbing sites.

In the first steps of the heating experiments, the band at 1885 cm^{-1} undergoes a consistent increase in the spectra (Fig. 1a), while a relatively small increase is observed on the reduced sample (Fig. 1b), indicating that nearly all of the few Cu(II) sites have already been engaged by NO, even at the low P_{NO} values present at the LNT. The most relevant spectroscopic feature observed in these spectra is the appearance of a new doublet at 1813 and 1717 cm^{-1} (strong in Fig. 1b and weak in Fig. 1a), which progressively grows with increasing P_{NO}. The spectral range and the separation of the two bands ($\Delta\nu = 96$ cm^{-1}) are typical of di-nitrosil complexes formed on cuprous ions (14, 21, 22); also the fact that they behave in a parallel way (as demonstrated by the constant ratio of the integrated area) supports this hypothesis. Conversely to what was observed for the 1885 cm^{-1} band, the doublet is much more intense after treatment with C_2H_4 (Fig. 1b).

The temperature-dependent IR experiment has been duplicated on the Cu0.25 sample. The results are visible in the full-line spectra reported in Fig. 2. From a first view of the two sets of full-line spectra, it is evident that sample Cu0.25

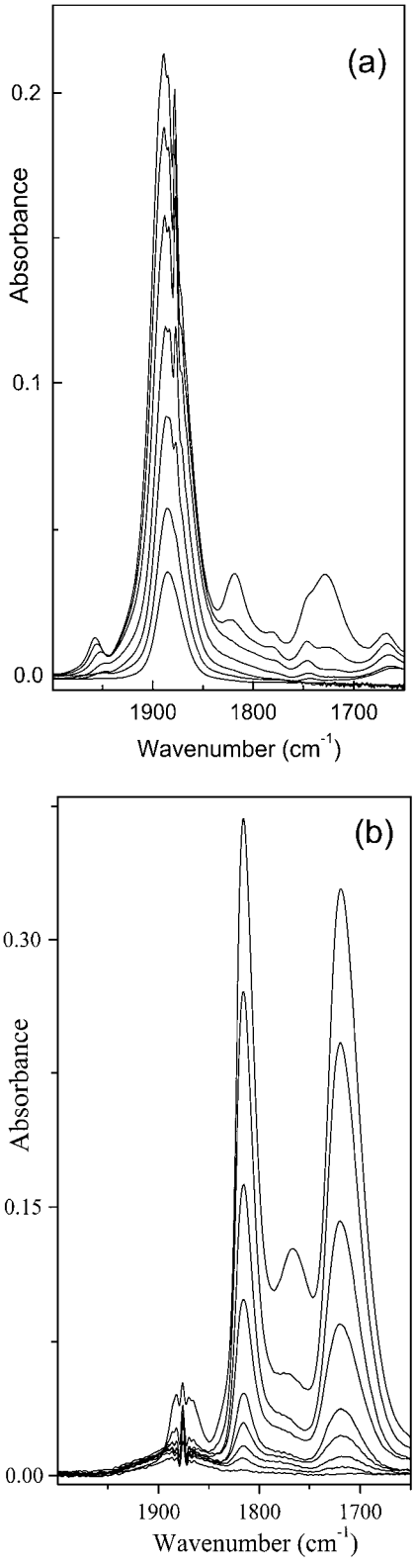

FIG. 1. IR spectra of NO on Cu9.0 (previously activated at 500 K) (a) before and (b) after interaction with ethylene at 500 K. The experiments show the effect of increasing the sample temperature from LNT up to the temperature resulting in the spectrum corresponding to the maximum intensity of the bands (see Section 2).

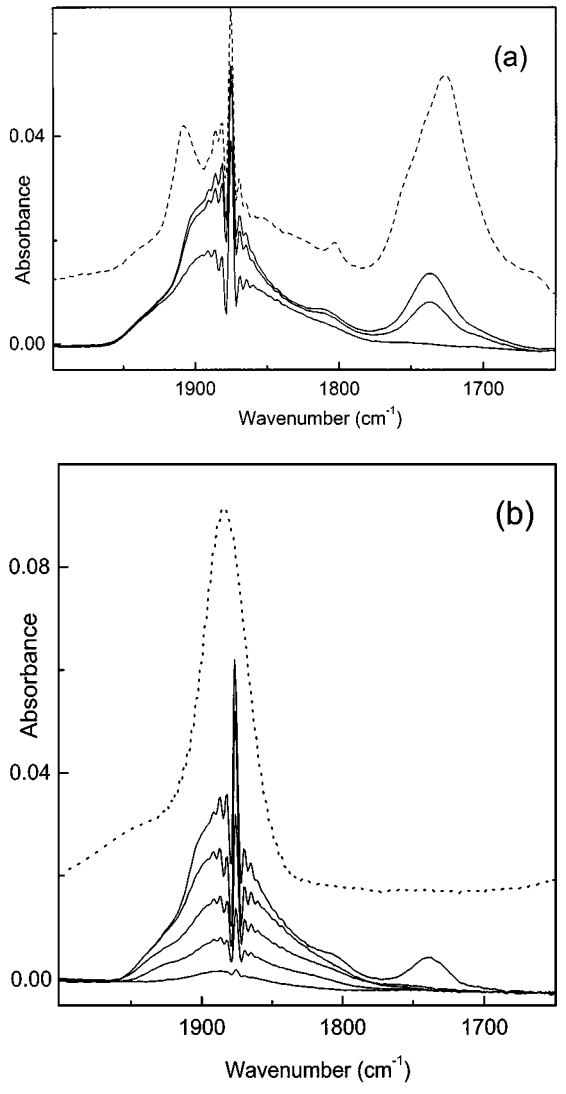

FIG. 2. Full-line spectra as in Fig. 1 for the Cu0.25 sample. The decrease of about 1 order of magnitude in the band intensities with respect to those reported in Fig. 1 is remarkable. The vertically translated dotted spectra represent the maximum coverage obtained in similar experiments, with (a) the bare γ-Al_2O_3 support calcined at 973 K and (b) on the Cu1.4 sample.

behaves in the same way before and after treatment with ethylene.

3.1.2. XANES study. The pre-edge region of X-ray absorption spectra can give direct information on the oxidation state of copper. In fact, it is widely recognized that Cu(II) species exhibit: (i) a weak absorption at about 8976–8979 eV, attributed to the dipole-forbidden 1s → 3d electronic transition; and (ii) a shoulder at about 8985–8988 eV and an intense peak at about 8995–8998 eV, both due to the dipole-allowed 1s → 4p transition (14, 18, 23–25). A single peak at 8983–8984 eV (due to 1s → 4p electronic transition) is the fingerprint of the Cu(I) species (14, 18, 23, 24).

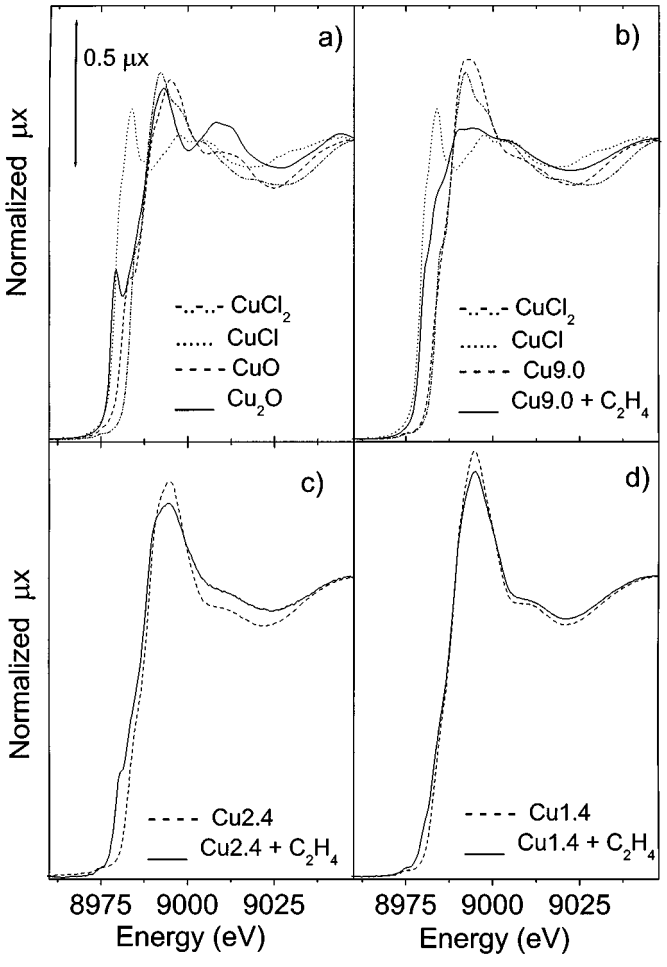

FIG. 3. (a) XANES spectra of $CuCl_2$, CuO, CuCl, and Cu_2O model compounds. Effect of interaction with ethylene at 500 K on the XANES spectra of (b) Cu9.0, (c) Cu2.4, and (d) Cu1.4 samples. In (b), the XANES spectra of $CuCl_2$ and the CuCl model compounds are also reported for comparison.

All these features are evident in the reference spectra of Cu(II) compounds (hydrated $CuCl_2$ and CuO) and Cu(I) compounds (anhydrous CuCl and Cu_2O) reported in Fig. 3a. The spectral shape after the edge (i.e., above 8995 eV) is different for the four compounds, reflecting a different local environment around copper in the four cases and resulting in a fingerprint of the compound.

Figures 3b–3d report the effect, on the XANES spectra, of the interaction with ethylene for Cu9.0, Cu2.4, and Cu1.4 samples, respectively. As far as sample Cu9.0 is concerned (Fig. 3b), a consistent red shift of about 4–5 eV is observed on sample activation and interaction with ethylene: this is clear evidence of the reduction of most copper ions present in the sample from Cu(II) into Cu(I) and of the absence of a measurable further reduction to the Cu(0) species [the edge of the Cu(0) species being expected about 2 eV below that of Cu_2O]. The presence of a small (less than about 15%) fraction of unreduced Cu(II) species is suggested by the presence of a minor inflection at around 8985 eV. The same experiment performed on sample Cu2.4 (Fig. 3c) yields a considerably lower reduction, indicating that after interaction with ethylene, a consistent fraction of copper is still in the oxidation state +2. Finally, the XANES spectra collected on sample Cu1.4 (Fig. 3d) indicate that the fraction of reduced Cu(II) species is, in this case, very small (a few percent).

3.1.3. NIR DRS and EPR study. The Cu(II) → Cu(I) reduction implies that the copper species modify their electronic configuration from $3d^9$ to $3d^{10}$. The modification causes the disappearance, in the near infrared (NIR) region, of the d–d transitions of the involved species and, in the microwave region, of a decrease of the electron spin flip transitions observed in the EPR spectra.

Figure 4 shows the d–d band of the Cu9.0 sample before and after interaction with C_2H_4. A remarkable decrease of the intensity of the d–d band is clearly observed in the reduced spectrum (dotted curve), which becomes very similar to the spectrum of sample Cu1.4, containing only the copper aluminate phase. The latter exhibits the same NIR diffuse reflectance spectroscopy (DRS) after interaction with ethylene (not reported for brevity).

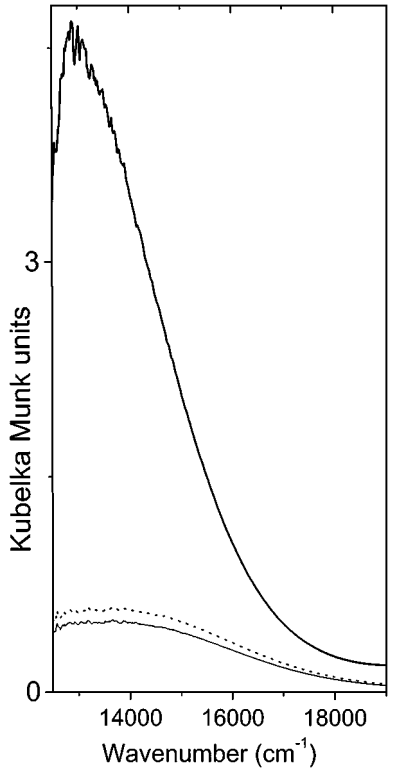

FIG. 4. NIR DRS spectra. From top to bottom: the Cu9.0 sample before and after interaction with C_2H_4 at 500 K and, for comparison, Cu1.4 before interaction with C_2H_4 (solid, dotted, and dashed lines, respectively). The first two spectra have been obtained after subtraction of the band due to charge transfer transitions, causing the brown color of the dehydrated catalyst (1, 2).

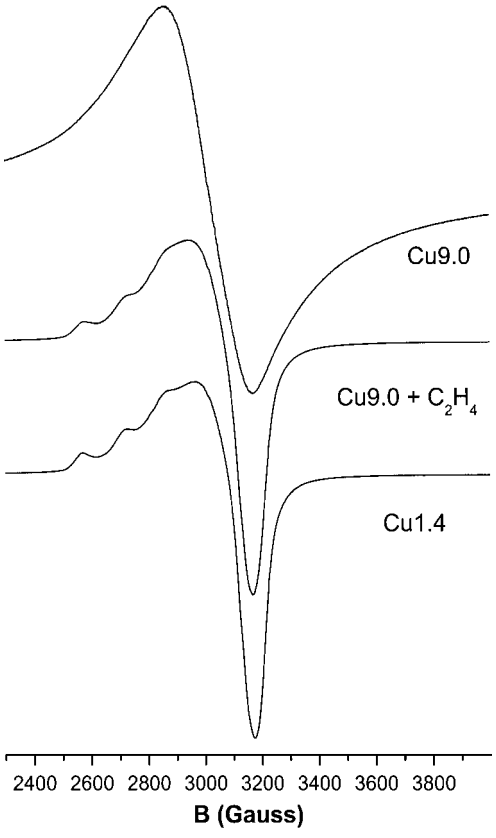

FIG. 5. EPR spectra collected at LNT. From top to bottom: Cu9.0 sample before and after interaction with C_2H_4 at 500 K and, for comparison, Cu1.4 before interaction with C_2H_4. Before cooling, samples were evacuated at room temperature up to 10^{-3} Torr.

Figure 5 reports the EPR spectra of anhydrous Cu9.0 before and after interaction with ethylene and the spectrum of sample Cu1.4 for comparison. The similarities of the last two spectra indicate that no EPR-detectable signal coming from $CuCl_2$ is present in the sample after interaction with ethylene. In contrast, exposure to ethylene of sample Cu1.4 leaves its EPR spectrum unaffected (not reported for brevity).

3.1.4. Concluding remarks on the reducibility of the copper species. From the whole set of the presented data it can be concluded that the two Cu(II) species present on the catalyst behave in a different way on interaction with ethylene: the supported $CuCl_2$ undergoes a reduction while the surface aluminate phase remains unreactive. This conclusion is in agreement with the activity tests performed in a pulse reactor on Cu9.0, Cu4.6, and Cu1.4 samples (2) showing that: (i) the Cu1.4 sample is inactive in ethylene conversion to dichloroethane; and (ii) the increase of activity observed in sample Cu9.0 with respect to sample Cu4.6 is not proportional to the ratio between the total amount of copper present in the two samples, but to the ratio between the amount of copper in the $CuCl_2$ phase.

The IR data show that nearly all the Cu(II) cations present at the surface of the $CuCl_2$ phase are reduced to Cu(I). The XANES study enhances our knowledge of the reduction process achieved by IR, showing that almost 80% of the total copper present in sample Cu9.0 is reduced after interaction with C_2H_4. This percentage corresponds to the fraction of copper present in the form of reactive $CuCl_2$ in sample Cu9.0, while the remaining fraction ($\approx$20%) is in the form of surface copper aluminate (see Section 1 and Ref. (1)). For sample Cu9.0 after interaction with ethylene, both EPR and NIR DRS experiments show a spectrum very similar to that observed on the Cu1.4 sample, which proves the nearly total elimination of the signal coming from (and only from) the Cu(II) ions in the $CuCl_2$ phase.

The complete reduction of copper chloride can be interpreted by supposing either a very high dispersion of $CuCl_2$ or an ability of ethylene to disgregate $CuCl_2$ particles or to extract bulk Cl^- from them. Of course each hypothesis does not exclude the others. In Section 3.3, we will discuss in more detail the dispersion of copper.

3.2. Nature of Reduced Copper Species: A XANES and EXAFS Study

In this section we look at determination of the Cu(I) species formed by reduction of $CuCl_2$. In Fig. 3b, the XANES spectra of anhydrous CuCl and hydrated $CuCl_2$ model compounds have been reported together with those of the Cu9.0 sample before and after interaction with ethylene for a direct comparison. The similarity in both edge position and shape of the spectrum of the as-prepared sample with that of $CuCl_2$ is a consequence of the fact that the dominant copper species present on freshly prepared, highly loaded samples is hydrated $CuCl_2$ (1, 2). Below 8980 and above 8995 eV, the same similarity also exists between the XANES spectra of the Cu9.0 sample after interaction with C_2H_4 and CuCl: this represents the first direct proof that the reduced copper species, present on the catalyst after interaction with ethylene, is dispersed CuCl. The fact that the white line (edge peak around 8983 eV) of the Cu9.0 sample after interaction with C_2H_4 is remarkably less intense and defined than the corresponding XANES feature of bulk CuCl can be ascribed to a marked difference in the higher shells around the Cu(I) species. Note that this behavior is exactly what is expected for highly dispersed CuCl particles, where only the oxidation state and the first coordination shell are comparable to those found in bulk CuCl.

To finally clarify this point, we present a detailed EXAFS data analysis of the Cu9.0 catalyst after reduction with ethylene proving that the fraction of copper in the active phase has a first coordination shell compatible with that of CuCl. To achieve this result a two-shell fit must be performed, because the EXAFS spectrum of the reduced Cu9.0 sample also contains the contribution of the Cu(II) species of the

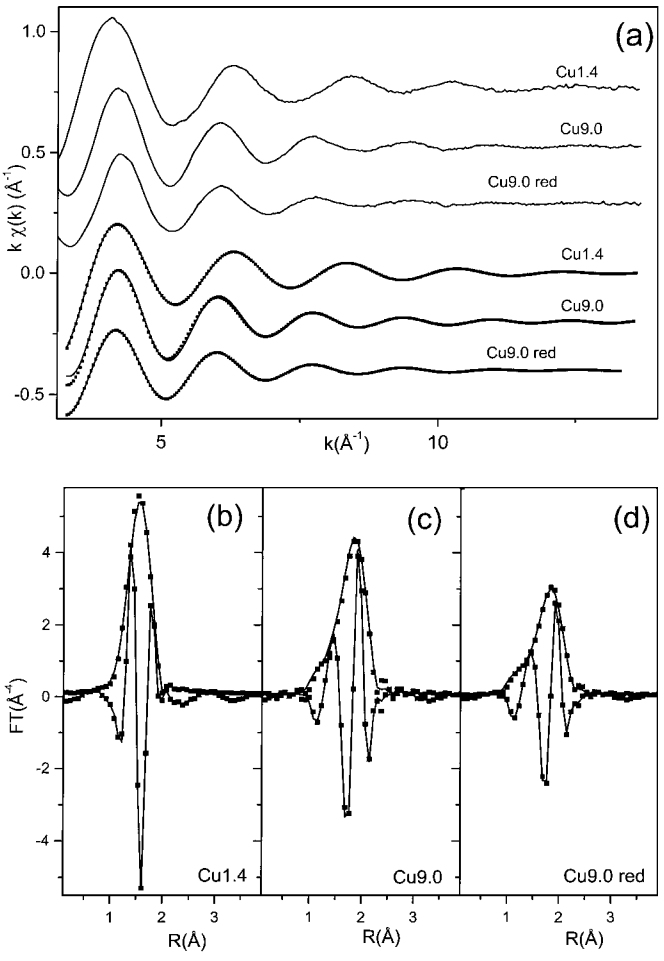

FIG. 6. From top to bottom: (a) raw EXAFS data of Cu1.4, Cu9.0 (both before interaction with C_2H_4), and Cu9.0 after interaction with C_2H_4 at 500 K, and corresponding best fits superimposed to the first shell-filtered signal. (b–d) The same fits in R space (both modulus and imaginary parts). No phase correction has been adopted.

copper aluminate phase, in which the local environment is not modified by interaction with ethylene. This means that once a careful one-shell fit is done on sample Cu1.4 (containing only the aluminate phase), the obtained coordination number, bond length, and Debye–Waller factor can be used as fixed parameters for the Cu–O shell of the fit done on sample Cu9.0.

Figure 6a reports the experimental $k\chi(k)$ function of Cu1.4, Cu9.0 before and after interaction with ethylene (first three spectra from top), and the first shell-filtered signal compared with the corresponding fit. The same fits are reported in R space in Figs. 6b–6d. As far as the Cu1.4 sample is concerned, we know that Cu(II) ions are hosted in the octahedral surface vacancies of γ-Al_2O_3 (1–3). A good fit has been obtained on sample Cu1.4 by fixing the coordination number N to 5 and by optimizing the Debye–Waller factor σ, the Cu–O distance R, and the energy shift ΔE. A further slight improvement of the fit has been obtained by optimizing the electron mean free path parameter γ that moves from the arbitrarily fixed value of $\gamma = 1.0$ to $\gamma = 0.7$ (Fig. 6a, fourth curve from the top, and Fig. 6b). The optimized R_{Cu-O} distance is 1.94 ± 0.01 Å, which is exactly half of the O–O distance in each couple of oxygen atoms diametrically opposite in an octahedral cationic site of the γ-Al_2O_3 spinel structure (26). Such sites are occupied by an Al^{3+}, but a fraction of them hosts a cationic vacancy that is occupied by cupric cations on impregnation with $CuCl_2$ (1). It is finally worth noticing that, if N is successively released, it converges to a value of 4.98.

Before trying the two-shell fit on the reduced Cu9.0 sample, where the nature of the reduced Cu phase is still unknown, we have tested it on the sample before interaction with ethylene, where both phases are known (1–3). According to the structural model described in Ref. (1), the amount of Cu(II) as surface Cu–aluminate and as dispersed $CuCl_2$ is 1.6 and 7.4 Cu wt% respectively, corresponding to relative fractions of 0.178 and 0.822. The expected coordination numbers (N_{exp}) have been fixed to structural coordination numbers (5 for Cu–aluminate and 4 for $CuCl_2$) multiplied by the relative fraction of the two species, resulting in N_{exp} equal to 0.89 and 3.29, respectively (see, e.g., Ref. 25). The quality of the fit obtained under such severe constraints (see second curves from the bottoms of Figs. 6a and 6c) validates the whole picture.

The result of this test justifies the application of the two–shell fit to sample Cu9.0 reduced in ethylene. In this case N_{exp} of the chlorine shell is left free because coordination of the Cu(I) ions in the reduced phase is unknown *a priori*. The results of the fit are summarized in Table 1: a bond length of 2.25 ± 0.02 Å and are N_{exp} value of 3.4 ± 0.2 have been found for the Cu–Cl shell. Considering that the fraction of Cu in the reduced phase is 0.822 of the total copper, the coordination number of Cu in this phase is $N = 4.14 \pm 0.24$, a value consistent with $N = 4$ of CuCl. Since the R value is reasonable, it is concluded that the Cu(I) species formed by reduction of $CuCl_2$ is CuCl.

Interaction with ethylene causes a consistent decrement of the EXAFS oscillations (compare the first $k\chi(k)$ functions from the bottom of Fig. 6a). This effect can also been observed comparing the corresponding k^3-weighted Fourier transform (FT) (Figs. 6c and 6d). The EXAFS data analysis (Table 1) shows that this reduction is not due to a decrement of the number of chlorine ligands in the first coordination shell of copper, but to an increase of the Debye–Waller factor. An important increase of σ, from 5.8×10^{-2} to 8.1×10^{-2} Å, cannot be explained by only a reduction in the Cu—Cl bond strength (expected as a consequence of the decrement of the ionic part of the cation–anion interaction), but must also be ascribed to a static effect, suggesting an increase of the particle dispersion caused by interaction with ethylene. The high dispersion achieved by the reduced phase is supported by data reported in Fig. 7, showing

TABLE 1

Filtering Ranges and EXAFS Results for First Coordination Sphere of the γ-Al_2O_3-Supported $CuCl_2$ Catalysts

Catalyst	Δk (Å^{-1})	ΔR (Å)	Shell	R (Å)	N	σ (10^{-2} Å)	ΔE (eV)
Cu1.4	3.34–14.31	1.07–1.84	Cu–O	1.94 ± 0.01	4.98 ± 0.25	5.8 ± 0.6	-1.1 ± 2.0
Cu9.0	2.93–14.09	0.96–1.96	Cu–O	1.94	0.89	5.8	-1.1
activated			Cu–Cl	2.25 ± 0.02	3.29	5.8 ± 1.1	-1.0 ± 2.0
Cu9.0	2.93–14.09	0.96–1.96	Cu–O	1.94	0.89	5.8	$+7 \pm 2.0$
reduced			Cu–Cl	2.25 ± 0.02	3.4 ± 0.2	8.1 ± 1.2	-2.0 ± 2.0

Note. Δk = interval of k-space to R-space FT; ΔR = R-space interval selected to perform the first shell-filtered back-FT into k-space; R = bond distance; N = coordination number; σ = relative Debye–Waller factor; ΔE = energy shifts. Nonoptimized parameters can be distinguished by the absence of corresponding error bars.

evolution of the XANES spectra (Fig. 7a), and the corresponding k^3-weighted phase uncorrected FT (Fig. 7b) of the reduced Cu9.0 catalyst on interaction with CO and NO. Both adsorbates modify the FT of the catalyst with the effect of NO absorption higher than that of CO. This fact can be explained by considering that carbon monoxide forms Cu(I)CO adducts while $Cu(I)(NO)_2$ adducts are formed on interaction with nitrous oxide (see corresponding IR studies in this paper). Quantitative EXAFS data analysis cannot be easily done because of the complexity of the samples in interaction with adsorbates; however, the important modifications observed on interaction with both probe molecules represent the direct, although qualitative, proof of the high dispersion of CuCl. The results discussed here introduce the topic of the dispersion of the active phase presented in the next section.

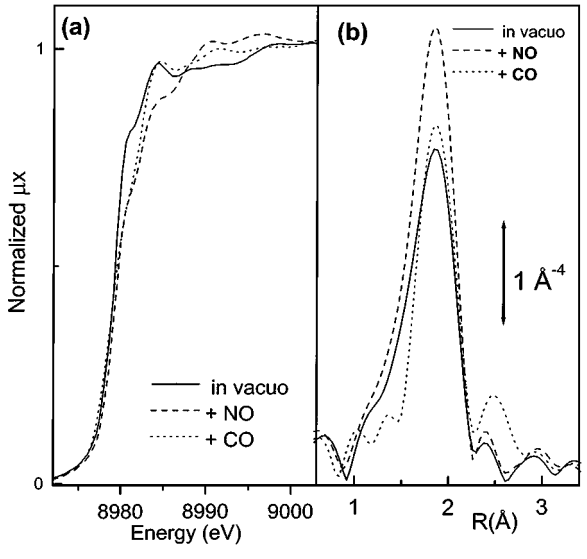

FIG. 7. Evolution of the XANES spectra (a) and the corresponding k^3-weighted phase uncorrected FT (b) of the reduced Cu9.0 catalyst on interaction with CO and NO.

3.3. Dispersion of Reduced Copper Species

3.3.1. IR Study of CO adsorbed on high Cu–loaded catalysts: low–frequency band. CO is an excellent probe molecule for Cu(I) sites (14, 27–30), because its interaction is normally rather strong. The interaction can be separated into an electrostatic, a covalent σ-dative, and a π-back donation contributions, the first two causing a blue shift of the ν(CO), while the last causes a red shift (31). From a measurement of the ν(CO) of a given Cu(I) carbonyl complex, information can be obtained on the nature of the Cu (I)—CO bond. In contrast, the interaction of CO with Cu(II) is very weak (32) and can be considered, in first approximation, negligible.

Figure 8 reports the IR spectra of increasing P_{CO} dosed at LNT on the Cu4.6 sample before (Fig. 8a) and after (Fig. 8b) interaction with ethylene. In both parts of the figure, the spectra are characterized by two distinct main absorptions. The high wavenumber one exhibits a maximum at 2158 cm^{-1}, independent of the CO coverage (θ) and sample treatment, while the band at lower frequency progressively shifts on increasing θ from 2135 cm^{-1} ($\theta \to 0$) to 2127 cm^{-1} (θ_{max}) in the unreduced sample (Fig. 8a). In the reduced sample (Fig. 8b) the singleton frequency ($\theta \to 0$) occurs at 2129 cm^{-1} while the frequency at θ_{max} cannot be determined owing to saturation of the band. On reduction, the high-frequency band is nearly unchanged, while the low-frequency band increases dramatically in intensity: this fact suggests that only the latter should be related to a species involved in the reduction process. In the following we will focus on the high-frequency band discussed in Section 3.4.1.

The low-frequency band—the only one present at the lower P_{CO}, the most resistant on evacuation, and the only one observed at RT (*vide infra*; see Fig. 10)—is ascribed to a Cu(I) . . . CO complex formed on CuCl dispersed on alumina. In a similar IR experiment, rather different frequencies, but comparable shift versus P_{CO}, have been obtained by Scarano *et al.* (29) on disordered CuCl growth by vapor-phase deposition on a NaCl(001) single crystal, where the

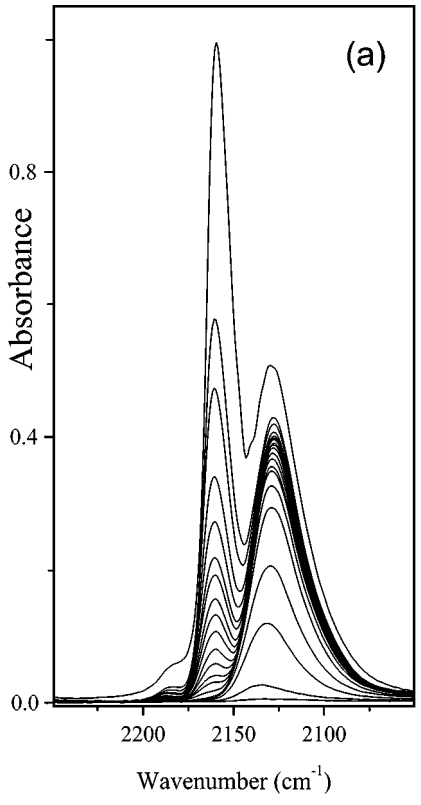

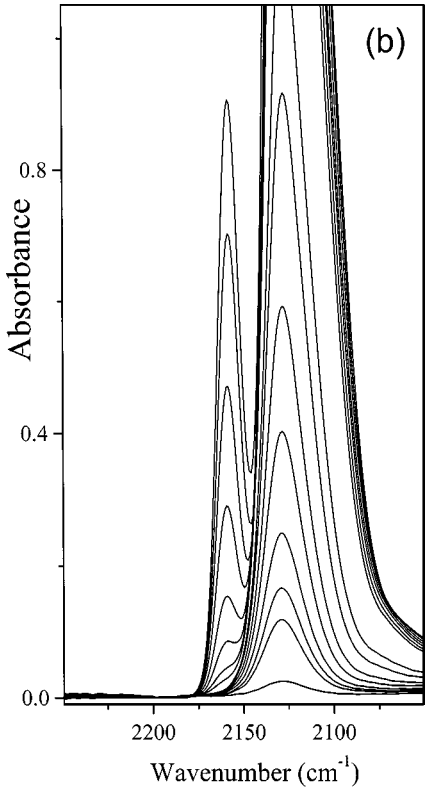

FIG. 8. IR spectra of increasing CO equilibrium pressures dosed, at LNT, on the Cu4.6 sample (previously activated at 500 K) (a) before and (b) after interaction with ethylene at 500 K.

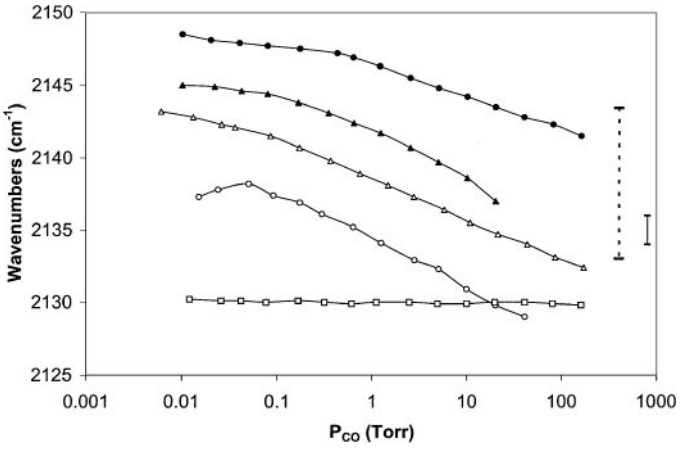

FIG. 9. Effect of the P_{CO} on the ν(CO) of the Cu(I)-specific IR band obtained on dosing CO at room temperature on Cu9.0 activated at 500 K (●), Cu9.0 reduced in ethylene at 500 K (○), Cu4.6 activated at 500 K (▲), Cu4.6 at 500 K reduced in ethylene (△), and on a Cu5.0 sample prepared on α-alumina and reduced in ethylene at 500 K (□). Vertical bars indicate the dispersion of ν(CO) in the experiments performed by Scarano *et al.* (29) on disordered CuCl particles on NaCl(001) (dashed line) and on well-defined CuCl crystals on NaCl(001) (solid line).

Cu(I) . . . CO complex exhibits a ν(CO) moving from 2143 ($\theta \rightarrow 0$) to 2133 cm^{-1} (θ_{max}). The differences of both $\theta \rightarrow 0$ and θ_{max} ν(CO) observed on the Cu4.6 catalyst (Fig. 8) and on disordered CuCl growth on NaCl(001) (29) can be explained by comparing the evolution of ν(CO) versus P_{CO} for different catalysts characterized by different Cu loading, treatment, and support. These data are summarized in Fig. 9.[3] A remarkable modification of the ν(CO) versus P_{CO} relationship by reduction in ethylene is observed (compare filled vs empty symbols). As far as the Cu9.0 sample is concerned, ν(CO) moves from 2148–2131 cm^{-1} to 2138–2129 cm^{-1} on reduction. If $CuCl_2$ is supported on a low-surface-area α-Al_2O_3 (□ symbols), on reduction in C_2H_4, a ν(CO) around 2130 cm^{-1} is obtained independently of P_{CO}. A similar constant behavior [ν(CO) = 2136 cm^{-1} ($\theta \rightarrow 0$) and 2134 cm^{-1}(θ_{max})] was observed by Scarano *et al.* (29) on well-defined CuCl crystals obtained by reducing the growth speed of CuCl deposited on NaCl(001). CuCl particles obtained in that way exhibited a high degree of crystallinity with a well-defined morphology: a scanning electron microscopic study evidenced the presence of elongated prisms of more than 1 μm exhibiting the (110) as the largely predominant exposed face. Similar behavior of copper chloride supported on α-Al_2O_3 and well-crystallized CuCl is not surprising, since the reduction of the surface area of the support yields to the generation of much bigger and

[3] It is worth noting that the nonperfect reproducibility of the ν(CO) frequencies observed for the activated samples disappears on reduction in ethylene. This fact can be ascribed to different degrees of reduction obtained on the just activated samples.

homogeneous copper chloride particles, which can be better compared with the perfect crystals studied in Ref. (29). The fact that the frequency of CO adsorbed on the two systems differs by 4 cm^{-1} at θ_{max} can be interpreted in terms of the role played by the support in the determination of the dominant exposed face(s).

The different behavior of ν(CO) versus P_{CO}, for (i) copper chloride supported on γ-Al_2O_3 and disordered CuCl deposited on NaCl(001) ($-8 < \Delta\nu < -14\ cm^{-1}$) and (ii) copper chloride supported on α-Al_2O_3 and well-crystallized CuCl deposited on NaCl(001) ($-2 < \Delta\nu < 0\ cm^{-1}$) gives information on the size of the copper chloride particle of the catalysts. Thus, it is worth recalling that the shift of ν(CO) versus P_{CO} is commonly observed on adsorbing CO on the surfaces of oxide or halide particles and reflects the concomitant presence of two distinct effects: $\Delta\nu = \Delta\nu_{stat} + \Delta\nu_{dyn}$ (33). The static component is due to the modification of an unengaged adsorbing site caused by the fact that one or more adjacent sites are engaged by CO; therefore, the successively adsorbed CO molecules probe a continuously different local situation. This interaction propagates mainly through the solid. The dynamic component is due to the progressive building up of lateral–lateral interaction among adsorbed oscillators. It propagates mainly through the space and needs rather large and regular surfaces to be effective. After a careful IR study performed using a $^{12}CO/^{13}CO$ (15/85) isotopic mixture, Scarano *et al.* (29) have revealed that the nearly null $\Delta\nu$, observed on well-crystallized CuCl, reflects the presence of a static and a dynamic shift of comparable magnitude operating in different directions: $\Delta\nu_{stat} = -13\ cm^{-1}$ and $\Delta\nu_{dyn} = +11\ cm^{-1}$. The $\Delta\nu$ values observed on the γ-Al_2O_3–supported catalysts (see Fig. 9) are of the same sign and order of magnitude as $\Delta\nu_{stat}$ observed on well-defined CuCl crystals. We interpret this fact as proof of the very small size of the CuCl particles supported on γ-alumina. In fact, for molecules strongly interacting with the surface sites (such as CO on cuprous cations), the static effect is nearly fully operative even when only the nearest surface neighbor sites are occupied, while the dynamic effect needs the presence of large surfaces to be active.

To verify this hypothesis, the IR experiments of Scarano *et al.* (29) with isotopic mixture have been repeated on the Cu4.6 sample activated at 500. Figure 10 reports the spectra obtained in the ^{12}C–O stretching region ($^{12}CO/^{13}CO$ mixture and pure ^{12}CO, Fig. 10a and Fig. 10b, respectively). Spectra presented in Fig. 10a show the splitting of the previously described bands in a less intense family (2150–2130 cm^{-1}) and in a more intense family (2090–2050 cm^{-1}) due to ^{12}CO and ^{13}CO oscillators, respectively. The less intense family of bands behaves, on increasing P_{CO}, in the same way it does when pure ^{12}CO is dosed, moving from 2141 cm^{-1}($\theta \to 0$) to 2134 cm^{-1}($\theta \to \theta_{max}$). This is proof that the dynamic effects play a negligible role in determining the

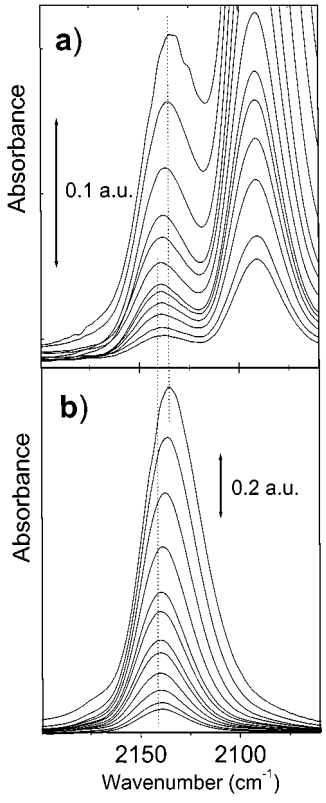

FIG. 10. (a) IR spectra of $^{12}CO/^{13}CO$ (15/85) isotopic mixture dosed at room temperature (increasing P_{CO} from 0.01 up to 40 Torr) on the Cu4.6 sample activated at 500 K (zoom over the ^{12}C–O stretching band). (b) Same as (a) for pure ^{12}CO.

ν(CO) versus P_{CO} relationship (which is thus mainly governed by static effects) and in turn implies that the size of the CuCl particles formed on the catalyst on reduction with ethylene is very small.

The small particle size implies a large heterogeneity of the adsorbing Cu(I) sites, which is reflected in an inhomogeneous broadening effect on the measured IR band showing extremely large FWHM (in the range of 20–30 cm^{-1}; see Figs. 8 and 10). For sake of comparison, FWHMs of 5–6 cm^{-1} are obtained on the high crystalline CuCl samples studied in Ref. (29). In conclusion, the surface area of the support, the amount of supported $CuCl_2$, and its degree of reduction affect the size and the shape of the supported CuCl particles, which in turn modulate the relative population of Cu(I) surface sites and thus the features (in particular, maximum frequency and FWHM) of the IR band obtained on probing surface sites by CO at different P_{CO}.

3.3.2. Quantitative measurements of adsorbed CO. The IR study on adsorbed CO leads to the conclusion that CO adsorbs only on Cu(I) sites at RT to form Cu(I)...CO adducts (Fig. 10). In fact, the minor IR features at 2157 and 2185 cm^{-1} (less than 0.1 in absorbance units) have been observed only at LNT (Fig. 8) and no vestige appears in the RT

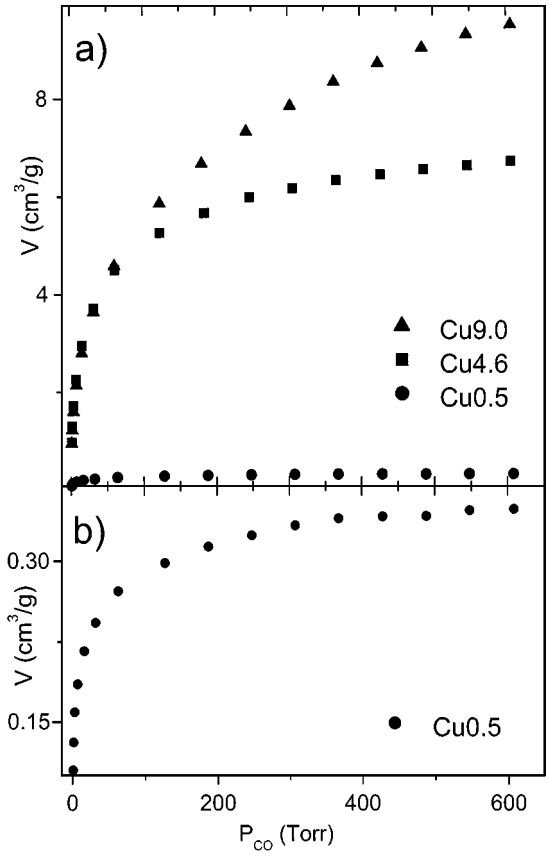

FIG. 11. (a) Volumetric data of CO adsorbed at room temperature on Cu9.0, Cu4.6, and Cu0.5 samples after interaction with ethylene at 500 K. (b) Magnification of the volumetric data of the Cu0.5 sample.

spectra. This fact justify the use of CO as a probe molecule to detect the number of surface Cu(I) sites by usual static-volumetric adsorption measurements (34). The adsorption isotherms of samples Cu9.0, Cu 4.6, and Cu0.5 are reported in Fig. 11. Before extracting quantitative information, the possible contribution to the total CO adsorption of (i) multiple adsorption on Cu(I), (ii) physisorption (unspecific adsorption or liquid-like CO), and (iii) adsorption on support must be evaluated to avoid a systematic overestimation of the copper dispersion.

To exclude the formation of dicarbonyls, IR spectra and volumetric adsorption data have been collected up to 600 Torr (Fig. 11). Up to 300 Torr, only a well-defined band is detectable with frequency that can be read with high accuracy up to 100–180 Torr (Fig. 9). Over 300 Torr, the top of the band is flat, owing to saturation, but traces of splitting due to dicarbonyl formation (14, 22, 27, 31, 32, 35) have not been observed. Moreover, this phenomenon has not been observed even in the LNT experiments (Fig. 8). Finally, the adsorption data reported in the Langmuir plot lie on a straight line from 70–150 to 600 Torr, without deviations in the high-pressure range.

In contrast, the role of physisorption cannot be excluded on the basis of IR measurements alone because the typical band, due to the physisorbed CO, should be observed around 2138 cm^{-1} (36): at high P_{CO} this band, if present, would be obscured by the much stronger adsorption due to Cu(I) . . . CO adducts (Figs. 8 and 10). Owing to the substantial nonselectivity of the physisorption process, it is usually quantified by means of adsorption measurements on the support (37, 38). The adsorption of CO on bare γ-alumina has been determined up to 600 Torr at 308 K, and very low values (0.0027 cm^3 m^{-2}; i.e., 0.07 molecules/nm^2) result. The same result (0.0029 cm^3 m^{-2}) has been obtained on chlorinated γ-alumina, indicating that the modification of the carrier surface undergone during the catalyst preparation does not change the support physisorption capacity. The effect of the surface area of the adsorbent has been investigated by comparing data obtained on γ-, $(\theta + \alpha)$-, and α-alumina samples. The adsorption per unit surface area is constant (third column in Table 2). In conclusion: (i) CO is physisorbed by all the supports in a low amount, more than an order of magnitude lower than the adsorption attributable to Cu(I) (Table 2); and (ii) the amount of physisorbed CO per unit surface area is substantially independent of the adsorbent surface with an average value of 0.00275 cm^3 m^{-2}. The difference among different supports (less than 0.0003 cm^3 m^{-2}) is about 1 order of magnitude lower than the total physisorption capacity of the supports (0.0026–0.0029 cm^3 m^{-2}) [i.e., 2 orders of magnitude lower than the total adsorption capacity of the catalysts (0.0424 cm^3 m^{-2} for Cu4.6 and 0.0660 cm^3 m^{-2} for Cu9.0]. On the basis of these results, the absorption due to Cu(I) . . . CO adduct has been obtained by subtracting the contribution of physisorption from total absorption: 0.00275 cm^3 m^{-2} multiplied by the surface area of the sample. The curves reported in Fig. 11 represent the corrected isotherms obtained on catalysts Cu9.0, Cu4.6, and Cu0.5.

TABLE 2

Volume of CO Adsorbed at 308 K and 500 Torr on Support and Modified Supports

Sample and treatment	Adsorbed volume (cm^3 g^{-1})	Surface area (m^2 g^{-1})	Adsorbed volume (cm^3 m^{-2})
Standard γ-alumina support	0.45	168	0.0027
Chorinated γ-alumina support	0.47	173	0.0029
Low-surface area $\theta + \alpha$-alumina support	0.08	32	0.0026
Low-surface-area α-alumina support	0.02	7.1	0.0028
Cu4.6 catalyst reduced in ethylene at 500 K	6.83	161	0.0424
Cu9.0 catalyst reduced in ethylene at 500 K	9.38	142	0.0660

Note. See text for details of sample preparations.

The isotherms show a slow increase of adsorbed volume with pressure. This does not allow evaluation of the adsorption volume correspondent to $\theta = 1$ by the usually adopted back extrapolation to 0 pressure and makes it necessary to analyze the isotherms with a proper model of the adsorption process (37). The Langmuir equation has given reliable results (Fig. 12) and was thus adopted to process experimental data. The equation is able to linearize data from 80–150 to 600 Torr for all catalysts. On these samples, having a large surface heterogeneity as probed by IR experiments (Figs. 8 and 10), CO occupies first the sites able to give a stronger interaction (low P_{CO} down-deviation of experimental data), while at higher pressure CO covers progressively the weaker and more uniform sites. In conclusion, the volume of the adsorbed CO correspondent to $\theta = 1$ (hereinafter V_m) can be evaluated by linearizing the adsorption isotherm with the Langmuir equation in the 150–600 Torr range. Knowledge of V_m allows calculation of the number of Cu(I) ions exposed to the surface ($Cu(I)_s$), and then the dispersion (D) can be calculated from

$$D = Cu(I)_s/Cu(I)_{tot}, \quad [5]$$

where $Cu(I)_{tot}$ represents the number of Cu(I) ions in the sample. A further evaluation leads to the estimation of the surface area of CuCl (S_{CuCl}),

$$S_{CuCl} = Cu(I)_s a_{CuCl}, \quad [6]$$

where a_{CuCl} (11.64 Å^2 as estimated from the chemical density, ρ_{CuCl}) is the average area per Cu(I) at the surface of CuCl. Table 3 summarizes the results obtained on Cu9.0, Cu4.6, and Cu0.5 samples. The low dispersion of the Cu0.5 sample is not surprising, since this sample contains only the unreactive surface aluminate phase and no supported $CuCl_2$ particles (1) and must be regarded as not meaningful. In contrast, Cu4.6 and Cu9.0 samples exhibit a high dispersion (0.455, 0.381). Even higher D values (0.715 and 0.468) are obtained by dividing $Cu(I)_s$ by the fraction of copper in the CuCl phase, which is the only one contributing significantly to the chemisorption process. The results quantify qualitative findings (XANES, EXAFS, and IR) on the very high Cu dispersion.

TABLE 3

Results of Static-Volumetric Measurements of CO Adsorption

Sample	V_m ($cm^3\ g^{-1}$)	D	S_{CuCl} ($m^2\ g^{-1}$)
Cu0.5	0.4	0.207	1.1
Cu4.6	7.4	0.455	23.1
Cu9.0	12.1	0.381	37.9
Cu4.6 corrected for Cu aluminate	7.4	0.715	23.1
Cu9.0 corrected for Cu aluminate	12.1	0.468	37.9

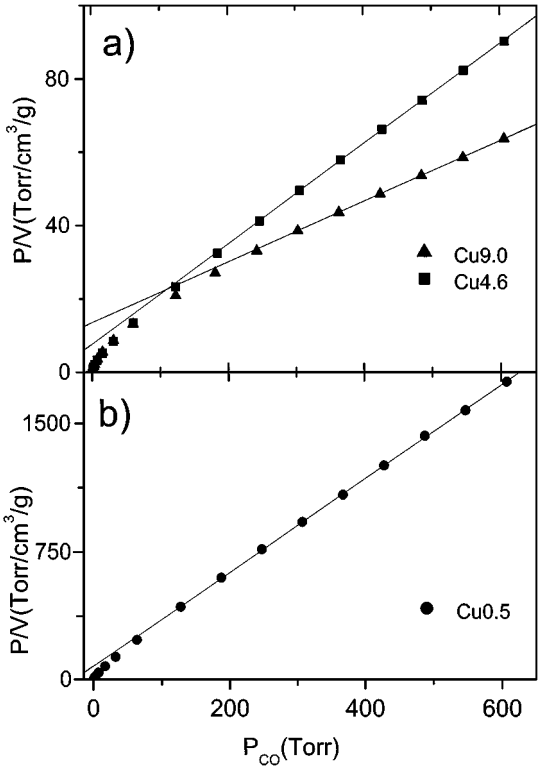

FIG. 12. Langmuir plots corresponding to the volumetric data of CO adsorbed on Cu9.0, Cu4.6, and Cu0.5 reported in Fig. 8. (a) Samples Cu9.0 and Cu4.6. (b) Sample Cu0.5.

3.3.3. On the formation of highly dispersed CuCl particles. CuCl present on the reduced catalyst has two different origins. The first part of CuCl (0–50%, depending on both Cu loading and aging of the sample (1, 2)) comes from reduction of $CuCl_2$, precipitated from the impregnating solution, and remained unchanged during sample aging. This fraction of $CuCl_2$ is already well dispersed as previously demonstrated (2), probably because of an interaction between precipitating salt and carrier surfaces. The reduction in ethylene causes an even higher dispersion measured by an increase of the Debye–Waller factor observed by EXAFS. The high dispersion of this fraction of CuCl ensures that it is spread onto the carrier surface with formation of quasi-monolayer islands or very small particles. The second part of CuCl (50–100%) comes from the reduction of rechlorinated paratacamite (2), which is present in relatively large crystals as demonstrated by the narrow peaks in the X-ray diffraction patterns of the aged samples (2). With the whole $CuCl_2$ present on activated samples that are highly dispersed, the rechlorination of paratacamite must cause: (i) spreading of the resulting $CuCl_2$ onto the carrier surface or (ii) formation of a large network of pores or cracks inside the large starting paratacamite particles, making most of them accessible from the outside. The following

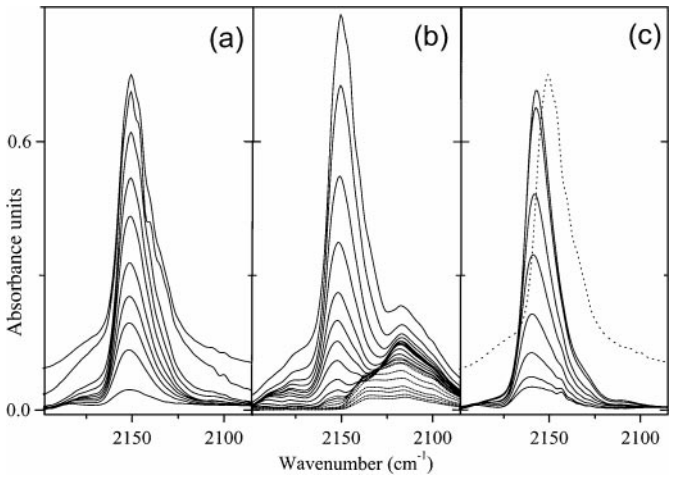

FIG. 13. IR spectra of CO dosed at LNT (increasing P_{CO} from 0.01 up to 20 Torr) (a) on the bare γ-Al_2O_3 support activated at 673 K, (b) on the copper surface aluminate formed from nitrates, and (c) on the chlorinated support. Vertically translated dotted spectrum reported in (c) is the high coverage band of (a), drawn here for comparison. Details on the sample preparation are reported in Section 2.

reduction to CuCl would not substantially modify this situation. The path which makes accessible the most CuCl is important because it affects the extent of interaction between the salt and the carrier, which likely affects its catalytic performance, the latter depending on whether CuCl is spread or forms large porous particles. At present, we are not able to draw an exhaustive picture of the distribution of CuCl on the carrier. Preliminary results of an already running work suggest that both spread and porous particles are present, depending on preparation and aging conditions.

3.4. *Nature Carrier-Free Surface*

3.4.1. IR study of CO adsorbed on high Cu-loaded samples: high-frequency band. Now we discuss the high-frequency band (2158 cm^{-1}) observed in the LNT IR spectra of all samples (Fig. 8 for Cu4.6). The assignment of this component has been done on the basis of LNT IR experiments on the bare γ-Al_2O_3 support, on a copper surface aluminate formed from nitrates and on the chlorinated support (Figs. 13a–13c).

The interaction of CO on γ-Al_2O_3 activated at 673 K (Fig. 13a) gives rise to a strong component centered at 2151 cm^{-1}, which is assigned to CO interacting with surface >Al–OH groups of alumina (39). A minor IR feature is also observed around 2185 cm^{-1} and will be ascribed to $>Al^{3+}\ldots(CO)$ adducts (*vide infra*; Section 3.4.2). When γ-Al_2O_3 is activated at 500 K, only the 2151 cm^{-1} component is present (not reported for brevity). The experiment performed on the sample prepared from nitrates (Fig. 13b) gives rise to two bands at 2151 cm^{-1} (broad) and 2117 cm^{-1} (very broad), ascribed, respectively, to >Al–OH . . . CO and Cu(I) . . . CO adducts formed at the surface of the copper aluminate phase.

The unassigned 2158 cm^{-1} band observed on catalysts is not affected by reduction with ethylene (Fig. 8) and has a similar pressure-dependent behavior of the 2151 cm^{-1} band observed on alumina and on the copper surface aluminate (Figs. 13a and 13b). On this basis, the 2158 cm^{-1} band is attributed to >Al–OH . . . CO adducts formed on the support. The different frequency position (2158 vs 2151 cm^{-1}) can be explained by the presence of chlorine atoms hosted on the alumina surface (1), which increase the Brønsted acidity of the surface >Al–OH groups. In fact, the chlorinated γ-Al_2O_3 exhibits a ν(CO) band at 2157 cm^{-1} (Fig. 13c). This result also implies that a significant fraction of the support is still accessible to CO even if it carries out a consistent amount of supported copper chloride.

3.4.2. IR study of CO adsorbed on low Cu-loaded catalysts. New information and confirmation of previous assignments will be extracted from the IR experiment performed by dosing CO at LNT on the Cu0.25 sample (Fig. 14). Three main bands at 2120 (the only component observed at low P_{CO}), 2151, and 2185 cm^{-1} have been observed. The spectra

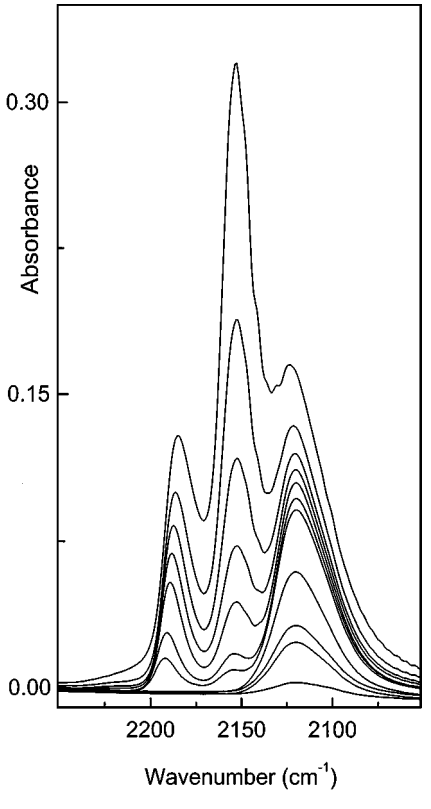

FIG. 14. IR spectra of increasing CO equilibrium pressure dosed at LNT on the Cu0.25 sample activated at 500 K. The corresponding experiment performed after interaction with ethylene (not reported) gives rise to the same spectra.

of the same experiment performed at RT (not reported for brevity) show the 2120 cm^{-1} component only: this allows the assignment of the band to Cu(I)...CO adducts formed on the small fraction of Cu ions of the copper aluminate phase reduced by the thermal treatment. The invariance of its ν(CO) on P_{CO} implies that we are dealing with isolated Cu(I) sites.

The band assigned to >Al–OH...CO adducts is detected at 2151 cm^{-1}, as on bare γ-Al_2O_3 and at a lower frequency than those observed on sample Cu4.6 or on the chlorinated support (2158 and 2157 cm^{-1}, respectively). This is because at low copper loading, the resulting small amount of chlorine anions hosted on the alumina surface is not able to significantly modify the acidic properties of the surface OH groups. If the same experiment is performed on the Cu1.4 catalyst, the C–O stretching band of the >Al–OH...CO adducts is observed at 2158 cm^{-1} (not reported for brevity).

The third band moves from 2193 to 2185 cm^{-1} on increasing P_{CO}. On the basis of the large amount of literature on the interaction of CO with the $>Al^{3+}$ Lewis sites on the surface of different aluminas (α, δ, γ, θ, and η) activated at different temperatures (39, 40), the 2185 cm^{-1} band is assigned to $>Al^{3+}$...(CO) adducts formed on Al^{3+} exhibiting only a partial coordinative unsaturation, like those occupying regular sites of the flat (110) surface of the γ-Al_2O_3 spinel. This explains why CO is able to adsorb on them at LNT only.

3.4.3. IR study of NO adsorbed on low Cu-loaded catalysts. IR spectra of NO dosed at LNT on Cu0.25 sample have been reported in Fig. 2 (solid lines). Due to the small Cu content, the intensity of the bands is 1 order of magnitude smaller than that observed for sample Cu9.0 in Fig. 1. The broad band, already detectable in the lowest P_{NO} spectra in the 1925–1850 cm^{-1} range, is tentatively ascribed to Cu(II)...NO complexes formed on the octahedral sites of the surface aluminate. Unfortunately, a fine study of this band (exact spectral location and FWHM measurement) cannot be done due to the its intrinsic weakness and the fact that the contribution of NO gas, absorbing in the same spectral region, is dominant. To verify the assignment, the same experiment has been repeated on the Cu1.4 sample. The spectrum at maximum intensity (Fig. 2b, dotted line) shows a band centered at 1883 cm^{-1} clearly emerging above the absorption due to NO in the gas phase, which is thus ascribed to Cu(II)...(NO). Also, the broad shoulder (around 1950 cm^{-1}) is more evident.

In the spectra of Cu0.25, on increasing P_{NO}, two additional components are detected: a well-defined band at 1737 cm^{-1} and a nearly unresolved shoulder around 1808 cm^{-1}. They appear in the wide spectral range where the adsorption of Cu(I)...NO and Cu(I)...$(NO)_2$ complexes are expected. However, the attribution to ν_{sym} and ν_{asym} of a single Cu(I)...$(NO)_2$ adduct is not feasible, because the ratio of the two integrated areas is not constant. To assign these bands, a parent experiment has been performed on the bare γ-Al_2O_3 support activated at 500, 773, and 973 K (dotted spectrum in Fig. 2a). The support activated at the same temperature as the catalyst (500 K) does not show any significant feature, while those activated at a higher temperature give rise to two defined absorptions at 1804 cm^{-1} (relatively weak) and at 1727 cm^{-1} (relatively strong), the intensities of which increase with temperature. The band at 1737 cm^{-1} and the shoulder around 1808 cm^{-1} are attributed to NO interacting with coordinatively unsaturated $>Al^{3+}$ Lewis sites located at the surface of the alumina crystals.

A shoulder around 1740 cm^{-1} is observed on dosing NO on the Cu9.0 sample (Fig. 1a). It demonstrates that, even on a sample with a high copper chloride loading, a significant fraction of the surface of the γ-Al_2O_3 support is still available for a small molecule such as NO. This conclusion confirms the discussion on the IR experiments of CO dosed at low temperature.

3.4.4. On the origin of the surface $>Al^{3+}$ Lewis sites. The presence of $>Al^{3+}$ groups on the catalyst needs some further clarifications. In fact, the surface of the bare γ-Al_2O_3 activated at 500 K is still fully covered by >AlOH groups, while coordinatively unsaturated $>Al^{3+}$ Lewis sites can be formed only after activation at a much higher temperature (39). On the catalysts the interaction between $CuCl_2$ and the hydroxylated alumina surface during impregnation gives an alternative pathway. According to Ref. (1), the following path has been put forward:

$$\begin{aligned} 2(>\text{Al–OH}) + CuCl_2 + 2(>\text{Al–OH}) &\rightarrow (>\text{Al–O})_2Cu \\ &+ 2HCl + 2(>\text{Al–OH}) \rightarrow (>\text{Al–O})_2Cu \\ &+ 2(>\text{Al–Cl}) + 2H_2O. \end{aligned} \quad [7]$$

The formation of a surface aluminate requires the appearance of Cu—O—Al bonds with elimination of chlorine, which, according to Eq. [7], is kept by alumina. Following the findings of Kytökivi *et al.* (41), in Ref. (1) we suggested that the reaction of $CuCl_2$ with alumina also induces the formation of >Al—Cl bonds because HCl is reacting with the surface as follows:

$$>\text{Al–OH} + HCl \rightarrow >\text{Al–Cl} + H_2O. \quad [8]$$

On activation at 500 K, part of the Cl anions hosted on the surface of alumina is released to reverse the $CuCl_2$ to paratacamite reaction (2). This in turn implies that also reaction [7] should be partially reversed; but, due to the lack of water in our experiments, the loss of a Cl^- implies the formation of coordinatively unsaturated $>Al^{3+}$ groups. The IR experiment performed by dosing CO on alumina impregnated with HCl and activated at 500 K (Fig. 13c) gives rise to only two components at 2158 and 2185 cm^{-1}, which definitively confirms our hypothesis.

It can be concluded that the surface of the catalyst activated at 500 K is rather complex because, in addition to the red-ox copper sites, also acidic sites of both Lewis ($>Al^{3+}$) and Brønsted ($>$Al–OH) nature are present and well accessible to both reactants and products. Of course, since the catalytic environment contains both HCl and H_2O, there is an equilibrium among the surface $>Al^{3+}$, $>$Al–OH, and the $>$Al–Cl species. These results point out the possible determinant role of the support in side reactions and coking, responsible for loss of selectivity and, catalyst decay respectively, during industrial runs.

4. CONCLUSIONS

The exposure to C_2H_4 at 500 K of a set of $CuCl_2/Al_2O_3$ catalysts, with a wide copper content range ($0.25 < Cu\ wt\% < 9.0$), has been investigated by means of XANES, EPR, NIR DRS, and EXAFS techniques and IR spectroscopy of adsorbed NO and CO. It has been demonstrated that the key mechanism of the oxychlorination reaction is the reduction of $CuCl_2$ to CuCl following the path $2CuCl_2 + C_2H_4 \rightarrow C_2H_4Cl_2 + 2CuCl$. The reaction holds for the totality of the cupric ions in the supported amorphous $CuCl_2$ phase. In contrast, Cu(II) cations belonging to the surface copper aluminate phase are unreactive toward ethylene. The CuCl phase formed after interaction of the catalysts with ethylene exhibits a very high degree of dispersion, up to 72%. Brønsted $>$Al–OH and Lewis $>Al^{3+}$ sites of the support surface are accessible to probe molecules even in the higher Cu-loaded catalyst (9.0 Cu wt%), suggesting their possible determinant role in the undesired side reactions and coking process, responsible for loss of selectivity and; catalyst decay during industrial runs.

APPENDIX

Comparison between Results from IR and Static-Volumetric Measurements of CO Adsorption Performed at RT

From the static-volumetric measurement of adsorbed CO at increasing P_{CO}, the amount of CO adsorbed versus P_{CO} has been obtained (Section 3.3.2). From the parallel RT IR experiments (Fig. 9), the area of the Cu(I)...CO-specific band has been determined at each P_{CO}. Combining data from the two experiments, it is possible to evaluate the trend of the extinction coefficient of the CO molecule forming Cu(I)...CO adducts at the surface of the catalyst versus P_{CO} (or coverage θ).

Figure 15 shows the trends obtained on Cu9.0 (1–60 Torr) and Cu4.6 (1–150 Torr) samples after reduction with ethylene. It is evident that the extinction coefficient is remarkably different for the two samples. This fact is not surprising, because in the whole P_{CO} range, the ν(CO) values observed on Cu9.0 lie below those measured on Cu4.6 (see ○ and △ symbols in Fig. 9), reflecting a greater π-backdonation in the Cu(I)...CO complexes formed on the Cu9.0 sample. This in turns implies a greater extinction coefficient for CO adsorbed on Cu9.0, in agreement with the combined IR and chemisorption data reported in Fig. 15.

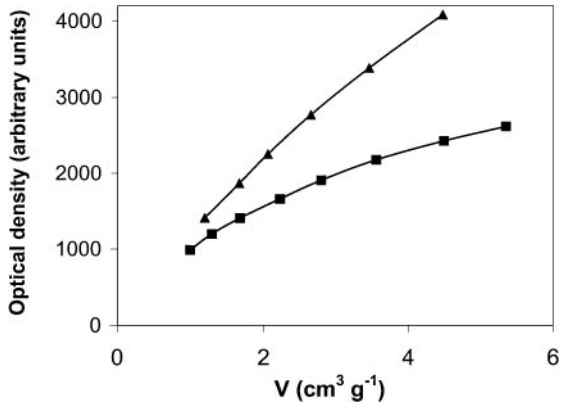

FIG. 15. Integrated IR bands vs RT CO adsorption isotherm on sample Cu9.0 (▲) and Cu4.6 (■) after interaction with ethylene at 500 K. Data refer to P_{CO} values ranging in the 1–60 and 1–150 Torr intervals for Cu9.0 and Cu4.6 catalysts, respectively.

For both samples, the evolution of the optical density versus the amount of adsorbed CO (i.e., vs coverage) deviates from linearity. The deviation is particularly evident in the first stages of adsorption. This behavior is that expected on the basis of the previously discussed chemisorption data, showing that the Langmuir model fits the experimental data in the high-P_{CO} region only (150–600 Torr). Data reported in Fig. 15 refer to the low-P_{CO} region of the chemisorption process where CO interacts with the energetically stronger Cu(I) sites, (i.e., those exhibiting higher heterogeneity). A linear trend, reflecting a constant extinction coefficient, is expected in the 150–600 Torr range but, due to the saturation of the IR bands, the region is not available for comparison.

This combined study underlies the fact that IR spectroscopy alone cannot be used to quantify the number of Cu(I)...CO adducts at the surface of the γ-Al_2O_3-supported $CuCl_2$ catalyst because the extinction coefficient of the CO molecule depends on (i) the amount of Cu loaded onto the catalyst, (ii) the degree of reduction of the catalyst, and (iii) the CO equilibrium pressure, at least in the P_{CO} range accessible to IR spectroscopy.

ACKNOWLEDGMENTS

We are deeply indebted to E. Giamello, G. Magnacca, D. Scarano, and G. Turnes Palomino for fruitful discussions and to F. Villain, F. Bonino, and A. Gabanotto for their relevant and friendly support during EXAFS measurements, with A.G. also acknowledged for performing chemisorption runs. Helpful comments of the referees are acknowledged.

REFERENCES

1. Leofanti, G., Padovan, M., Garilli, M., Carmello, D., Zecchina, A., Spoto, G., Bordiga, S., Turnes Palomino, G., and Lamberti, C., *J. Catal.* **189**, 91 (2000).
2. Leofanti, G., Padovan, M., Garilli, M., Carmello, D., Marra, G. L., Zecchina, A., Spoto, G., Bordiga, S., and Lamberti, C., *J. Catal.* **189**, 105 (2000).
3. (a) Casali, G., Cremaschi, B., Spoto, G., Carmello, D., Lamberti, C., Leofanti, G., and Zecchina, A., Presented at EUROPA-CAT-4, Rimini (I), 5–10 September 2000; (b) Garilli, M., Carmello, D., Cremaschi, B., Leofanti, G., Padovan, M., Zecchina, A., Spoto, G., Bordiga, S., and Lamberti, C., Presented at ICC-11, Granada (S), 9–14 July 2000; *Stud. Surf. Sci. Catal.* **130**, 1917 (2000).
4. Naworski, J. S., and Evil, E. S., *Appl. Ind. Catal.* **1**, 239 (1983).
5. Allen, J. A., *J. Appl. Chem.* **12**, 406 (1962).
6. Carrubba, R. V., and Spencer, J. L., *Ind. Eng. Chem. Proc. Dev.* **9**, 414 (1970).
7. Arganbright, R. P., and Yates, W. F., *J. Org. Chem.* **27**, 1205 (1962).
8. Rollins, K., and Sermon, P. A., *J. Chem. Soc. Chem. Commun.* 1171 (1986).
9. Dmitrieva, M. P., Bahshi, Yu. M., and Gel'bshtein, A. I., *Kinet. Katal.* **31**, 894 (1990).
10. Leofanti, G., Marsella, A., Cremaschi, B., Garilli, M., Zecchina, A., Spoto, G., Bordiga, S., Fisicaro, P., Prestipino, C., and Lamberti, C., submitted for publication.
11. Lamberti, C., Zecchina, A., Bordiga, S., Spoto, G., Leofanti, G., and Garilli, M., Proposal CK 017-00 LURE, Orsay (F), XAFS13 (D42), September 11–15, 2000.
12. Michalowicz, A., *J. Phys. IV (France)* **7**, C2-235 (1997).
13. (a) Lytle, F. W., Sayers, D. E., and Stern, E. A., *Physica B* **158**, 701 (1989); (b) Durham, P. J., *in* "X-Ray Absorption" (D. C. Koningsberger and R. Prins, Eds.), p. 53. Wiley, New York, 1988.
14. Lamberti, C., Bordiga, S., Salvalaggio, M., Spoto, G., Zecchina, A., Geobaldo, F., Vlaic, G., and Bellatreccia, M., *J. Phys. Chem. B* **101**, 344 (1997).
15. Burns, P. C., and Hawthorne, F. C., *Am. Mineral.* **78**, 187 (1993).
16. Restori, R., and Schwarzenbach, D., *Acta Crystallogr. B* **42**, 201 (1986).
17. (a) Li, Y., and Keith Hall, W., *J. Catal.* **129**, 202 (1991); (b) Sàrkàny, J., d'Itri, J. L., and Sachtler, W. M. H., *Catal. Lett.* **16**, 241 (1992); (c) Keith Hall, W., and Vaylon, J., *Catal. Lett.* **15**, 311 (1992); (d) Valyon, J., and Keith Hall, W., *J. Phys. Chem.* **97**, 7054 (1993); (e) Larsen, S. C., Aylor, A., Bell, A. T., and Reimer, J. A., *J. Phys. Chem.* **98**, 11533 (1994); (f) Jong, H. J., Keith Hall, W., and d'Itri, J. L., *J. Phys. Chem.* **100**, 9416 (1996); (g) Cheung, T., Bhargava, S. K., Mobday, M., and Foger, K., *J. Catal.* **158**, 301 (1996); (h) Lo Jacono, M., Fierro, G., Dragone, R., Feng, X., d'Itri, J., and Keith Hall, W., *J. Phys. Chem B.* **101**, 1979 (1997); (i) Dossi, C., Fusi A., Moretti, G., Recchia, S., and Psaro, R., *Appl. Catal. A* **188**, 107 (1999); (j) Dossi, C., Recchia, S., Pozzi, A., Fusi, A., Dalsanto, V., and Moretti, G., *Phys. Chem. Chem. Phys.* **1**, 4515 (1999).
18. (a) Grünert, W., Hayes, N. W., Joyner, R. W., Shpiro, E. S., Rafiq, M., Siddiqui, H., and Baeva, G. N., *J. Phys. Chem.* **98**, 10832 (1994); (b) Kuroda, Y., Yoshikawa, Y., Konno, S., Hamano, H., Maeda, H., Kumashiro, R., and Nagao, M., *J. Phys. Chem.* **99**, 10621 (1995); (c) Bolis, V., Maggiorini, S., Meda, L., D'Acapito, F., Turnes Palomino, G., Bordiga, S., and Lamberti C., *J. Chem. Phys.* **113**, 9248 (2000).
19. Giamello, E., Murphy, D., Magnacca, G., Morterra, C., Shioya, Y., Nomura, T., and Anpo, M., *J. Catal.* **136**, 510 (1992).
20. Turnes Palomino, G., Fisicaro, P., Giamello, E., Bordiga, S., Lamberti, C., and Zecchina, A. *J. Phys. Chem. B* **104**, 4064 (2000).
21. (a) Li, Y., and Hall, W. K., *J. Phys. Chem.* **94**, 6145 (1990); (b) Spoto, G., Bordiga, S., Scarano D., and Zecchina, A., *Catal. Lett.* **13**, 39 (1992); (c) Hadrjiivanov, K., and Knözinger, H., *Phys. Chem. Chem. Phys.* **3**, 1132 (2001).
22. (a) Turnes Palomino, G., Bordiga, S., Zecchina, A., Marra, G. L., and Lamberti, C., *J. Phys. Chem. B* **104**, 8641 (2000); (b) Spoto, G., Zecchina, A., Bordiga, S., Ricchiardi, G., Martra, G., Leofanti, G., and Petrini, G., *Appl. Catal. B* **3**, 151 (1994).
23. (a) Kau, L. S., Spira-Solomon, D. J., Penner-Hahn, J. E., Hodgson, K. O., and Solomon, E. I., *J. Am. Chem. Soc.* **109**, 6433 (1987); (b) Kau, L. S., Hodgson, K. O., and Solomon, E. I., *J. Am. Chem. Soc.* **111**, 7103 (1989); (c) Blackburn, N. J., Strange, R. W., Reedijk, J., Volbeda, A., Farooq, A., Karlin, N. D., and Zubieta, J., *Inorg. Chem.* **28**, 1349 (1989); (d) Reedy, B. J., and Blackburn, N. J., *J. Am. Chem. Soc.* **116**, 1924 (1994).
24. Lamberti, C., Spoto, G., Scarano, D., Pazé, C., Salvalaggio, M., Bordiga, S., Zecchina, A., Turnes Palomino, G., and D'Acapito, F., *Chem. Phys. Lett.* **269**, 500 (1997).
25. Turnes Palomino, G., Bordiga, S., Zecchina, A., Marra, G. L., and Lamberti, C., *J. Phys. Chem. B* **104**, 8641 (2000).
26. Zhou, R.-S., and Snyder, R. L., *Acta Crystallogr. B* **47**, 617 (1991).
27. Giamello, E., Murphy, D., Magnacca, G., Morterra, C., Shioya, Y., Nomura, T., and Anpo, M., *J. Catal.* **136**, 510 (1992).
28. (a) Scarano, D., Ricchiardi, G., Bordiga, S., Galletto, P., Lamberti, C., Spoto, G., and Zecchina, A., *Faraday Discuss.* **105**, 119 (1996); (b) Zecchina, A., Bordiga, S., Salvalaggio, M., Spoto, G., Scarano, D., and Lamberti, C., *J. Catal.* **173**, 540 (1998); (c) Scarano, D., Bordiga, S., Lamberti, C., Spoto, G., Ricchiardi, G., Zecchina, A., and Otero Areán, C., *Surf. Sci.* **411**, 272 (1998); (d) Zecchina, A., Bordiga, S., Turnes Palomino, G., Scarano, D., Lamberti C., and Salvalaggio, M., *J. Phys. Chem. B* **103**, 3833 (1999); (e) Lamberti, C., Turnes Palomino, G., Bordiga, S., Berlier, G., D'Acapito, F., and Zecchina, A., *Angew. Chem. Int. Ed. Engl.* **39**, 2138 (2000).
29. Scarano, D., Galletto, P., Lamberti, C., de Franceschi, R., and Zecchina, A., *Surf. Sci.* **387**, 236 (1997).
30. Zecchina, A., Scarano, D., Spoto, G., Bordiga, S., Lamberti C., and Bellussi, G., *Stud. Surf. Sci. Catal.* **117**, 343 (1998).
31. Strauss, S. H., *J. Chem. Soc. Dalton Trans.* 1 (2000).
32. Hadjiivanov, K., and Knözinger, H., *J. Catal.* **191**, 480 (2000).
33. (a) Hammaker, R. A., Francis, S. A., and Eischens, R. P., *Spectrochim. Acta* **21**, 1295 (1965); (b) Zecchina, A., Scarano, D., Bordiga, S., Spoto, G., and Lamberti, C., *Adv. Catal.*, in press (2001); (c) Zecchina, A., Scarano, D., Bordiga, S., Ricchiardi, G., Spoto, G., and Geobaldo, F., *Catal. Today* **27**, 403 (1996); (d) Zecchina, A., Scarano, D., and Bordiga, S., *in* "Handbook of Heterogeneous Catalysis" (G. Ertl, H. Knözinger, and J. Weitkamp, Eds.), Vol. 2, p. 728. Wiley-VCH, New York, 1997.
34. (a) Nag, N. K., *Catal. Lett.* **24**, 37 (1994); (b) Labalme, V., Benhamou, N., Guilhaume, N., Garbowski, E., and Primet, M., *Appl. Catal. A: General* **133**, 351 (1995).
35. Bolis, V., Maggiorini, S., Meda, L., D'Acapito, F., Turnes Palomino, G., Bordiga, S., and Lamberti, C., *J. Chem. Phys.* **113**, 9248 (2000).
36. (a) Bordiga, S., Escalona Platero, E., Otero Areán, C., Lamberti, C., and Zecchina, A., *J. Catal.* **137**, 179 (1992); (b) Lamberti, C., Morterra, C., Bordiga, S., Cerrato, G., and Scarano, D., *Vib. Spectrosc.* **4**, 273 (1993); (c) Bordiga, S., Scarano, D., Spoto, G., Zecchina, A., Lamberti C., and Otero Areán, C., *Vib. Spectrosc.* **5**, 69 (1993); (d) Gruver, V., Panov, A. and Fripiat, J. J., *Langmuir* **12**, 2505 (1993).
37. Bergeret, G., and Gallezot, P., *in* "Handbook of Heterogeneous Catalysis" (G. Ertl, H. Knözinger, and J. Weitkamp, Eds.), Vol. 2, p. 439. VCH, Weinheim, 1977, and reference therein.
38. Bozon-Verduraz, V., Tessier, D., and Rakai, A., *J. Catal.* **127**, 457 (1991).

39. Morterra, C., and Magnacca, G., *Catal. Today* **27**, 497 (1996) and references therein.
40. (a) Zecchina, A., Escalona Platero, E., and Otero Areán, C., *J. Catal.* **107**, 244 (1987); (b) Zaki, M. I., and Knözinger, H., *Spectrochim. Acta A* **43**, 1455 (1987); (c) Ballinger, T. H., and Yates, J. T. Y., Jr., *Langmuir* **7**, 3041 (1991); (d) Marchese, L., Bordiga, S., Coluccia, S., Martra, G., and Zecchina, A., *J. Chem. Soc. Faraday Trans.* **89**, 3483 (1993); (e) Morterra, C., Magnacca, G., and Del Favero, N., *Langmuir* **9**, 642 (1993); (f) Morterra, C., Bolis, V., and Magnacca, G., *Langmuir* **10**, 1812 (1994); (g) Morterra, C., and Magnacca, G., *Phys. Chem. Chem. Phys.* **2**, 3903 (2000).
41. Kytökivi, A., Lindblad, M., and Root, A., *J. Chem. Soc. Faraday Trans.* **91**, 941 (1995).